Sputter yield amplification by tungsten doping of Al2O3 employing reactive serial co-sputtering: process characteristics and resulting film properties

M Austgen, D Koehl, P Zalden, T Kubart, T Nyberg, A Pflug, M Siemers, S Berg, M Wuttig

Sputter yield amplification by Tungsten doping of Al_2O_3 employing reactive serial co-sputtering: process characteristics and resulting film properties

M Austgen[1], D Koehl[1], P Zalden[1] T Kubart[2], T Nyberg[2], A Pflug[3], M Siemers[3], S Berg[2] and M Wuttig[1,4]

[1] Institute of Physics (IA), RWTH Aachen University, 52056 Aachen, Germany
[2] Solid State Electronics, The Ångström Laboratory, Uppsala University, Box 534, 751 21 Uppsala, Sweden
[3] Fraunhofer IST, 38108 Braunschweig, Germany
[4] JARA-FIT, RWTH Aachen University, 52056 Aachen, Germany

Corresponding author: wuttig@physik.rwth-aachen.de, Phone: +49 (0) 241 80 27155, Fax: +49 (0) 241 80 22331

Abstract. The deposition rate of reactively sputtered Al_2O_3 coatings is demonstrated to increase by 80% upon Tungsten doping of the Aluminum target utilized. This effect is based on the recoil of the sputtering species at implanted dopants below the target surface and is termed Sputter Yield Amplification. For the investigation of this effect, a novel type of magnetron sputter deposition system has been employed that facilitates serial co-sputtering. In this technique doping of the elementary target is enabled by a dynamic sputtering process from an auxiliary cathode. In our case, the rotating Aluminum target has been dynamically coated with Tungsten from this auxiliary cathode. Since the primary target rotates, the auxiliary cathode is placed in series with the primary erosion zone. The deposition rate of Al_2O_3 can be considerably increased in this process already for very low concentrations of approximately 1% of Tungsten in the resulting film. A characterization of the dynamics of reactive sputtering as a function of target rotation speed has been performed.

Keywords. co-sputtering, serial co-sputtering, sputter yield amplification, rate enhancement, Al_2O_3

1. Introduction

Sputtering technology is widely used for many applications in the thin film coating industry. This is due to the excellent scalability of the process which enables homogeneous large area coating for e.g. next generation thin film solar cells or architectural glazing. The composition of the resulting films is only limited by the fabrication of the required targets if a single target is used for the deposition of the desired layer. However, in particular the deposition of metal oxides is often hampered by a very low deposition rate if the sputtering process is operated in compound mode. This low deposition rate is a characteristic feature of all metal oxides with a significantly higher binding energy than the corresponding metal [1]. Hence metal oxides with a high heat of formation such as alumina or Titanium dioxide have very low deposition rates. Hence, it is desirable to find ways to increase the deposition rate. The most promising attempts to increase the deposition rate of metal oxides will be summarized in the following. Some of these concepts feature disadvantages that inhibit their utilization in the large area coating industry. [2]

- **Nitride targets.** The erosion rate of a metal nitride surface is typically larger than that of the corresponding oxide. It has been demonstrated that the addition of nitrogen in a reactive sputtering process can increase the erosion rate. This is a consequence of the lower heat of formation of metal nitrides compared with the corresponding oxides which leads to a higher removal rate of the

nitride target. It is possible to operate the discharge at parameters that yield a partially nitridic target surface. The sputtered nitride, however, can be oxidized at the substrate due to the higher reactivity of oxygen with the metal. A significant rate enhancement by a factor of 1.3 is achieved by depositing TiO_2 from a TiN target which is sputtered in a reactive Ar/O_2 atmosphere. [3][4]

- **Hot target.** Sputtering from a hot target is possible by tailoring the cathode and cooling design. Heating of the target can stabilize the transition regime between the metal and the compound which is often unstable in reactive sputtering. Therefore, deposition in the transition regime at high erosion rates is possible which increases the deposition rate. [5][6][7]
- **HiPIMS.** It has been shown that under certain circumstances and for some materials the reactive discharge can be stabilized in the transition region without additional process control. Hence, it is possible to increase the deposition rate of reactive deposition processes by the choice of a working point in the transition regime [8][9]. However, the utilization of this technique on large cathodes, such as required by the large area coating industry, is technically challenging.
- **Incorporation of heavy ions.** This is a kinetic approach based on slight modifications of the target composition. During conventional sputtering, only a small fraction of the impinging ion's momentum gets reflected towards the target surface and causes sputtering, while the major fraction of the ion energy dissipates inside the target volume, where it adds to the thermal load of the target. Upon incorporation of heavy atoms into the target, e.g. Al:W or Ti:Bi, the heavy dopants act as recoil centers. Consequently a larger fraction of the collision cascade initiated by the impinging ions gets reflected towards the surface; thus the sputtering rate per impact power density is increased. [10][11]

The latter concept is subject to technical limits since the melting points e.g. of Ti and Bi are very different, rendering the fabrication of alloy targets very difficult. Hence, material mixing is more easily realized by a co-deposition process. The proof of this concept has been demonstrated in a dual ion beam sputtering setup [10], which is unsuitable for large area coatings. Subsequently the concept of sputter yield amplification (SYA) has been applied to magnetron sputtering processes. By simulations it has been demonstrated to be practicable most flexibly in a process known as serial co-sputtering (figure 1 A) [12][13]. The advantage of this process is that alloying of arbitrary compounds can be dynamically achieved by combining the respective elemental targets. Hence there are no limitations concerning both the choice of elements and the stoichiometry that can be realized. This work will focus on the SYA for Al_2O_3 sputtered by serial co-sputtering, since there already have been investigations in experiments and in modeling of reactive sputtering of Al by other groups [12][14][15][16][17]. Al and Al_2O_3 films have been deposited from Al and Al:W target surfaces in a reactive mode to investigate the deposition rate at different working points. The sputtering power of the Tungsten target, which will henceforth be denoted P_W, has been varied to control the concentration of Tungsten on the Al:W target surface. Furthermore, different rotation speeds of the Aluminum target have been applied to study the influence on the overall process behavior and the deposition rates. The concentration of Tungsten in the deposited films has been measured to confirm that the increase in deposition rate is mainly due to the increased erosion rate of the Aluminum compound.

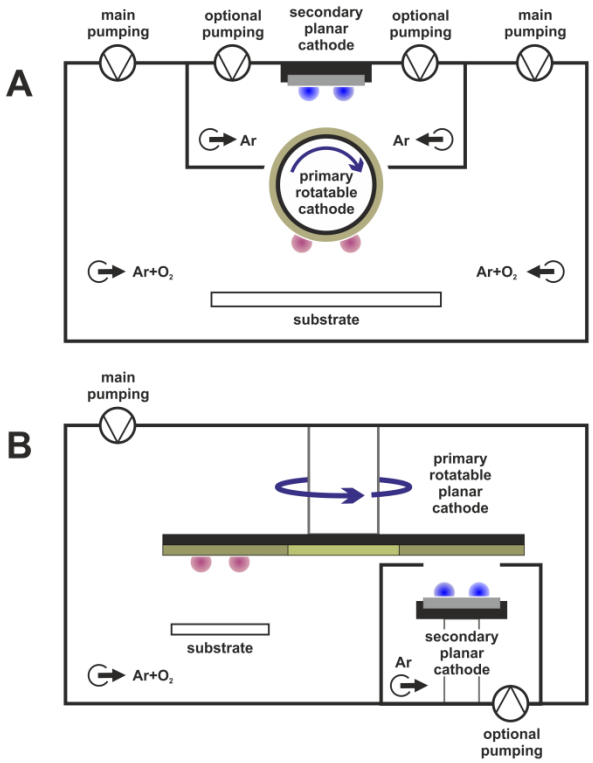

Figure 1. (A) Serial co-sputtering concept based on a cylindrical rotating target: Material A will be sputtered from the secondary cathode and deposited onto the rotating primary target consisting of material B. In a simultaneous sputtering process the A-doped material B will be deposited onto substrates. A gas shielding of the secondary process will allow serial co-sputtering in separated and almost independent atmospheres. **(B)** Concept based on a planar rotating target.

2. Experimental Details

2.1. Development of the lab coater

To investigate the serial co-sputtering process a new lab coater has been designed and constructed. The basic operation principle is similar to that shown in figure 1 A, but with a planar rotating disc target instead of a cylindrical target (figure 1 B). From the secondary source the additive material is non-reactively sputter deposited onto the primary rotating planar target. This results in a mixed elemental composition of the target surface that is subsequently sputtered in the primary erosion area. The diameter of the target is 300 mm and the rotation speed can be precisely adjusted between 1 and 35 rpm by a stepper motor. Two 76 mm planar auxiliary cathodes have been installed to enhance flexibility. Therefore the system consists of three separate chamber volumes. Both auxiliary cathodes can be operated in a pure Argon atmosphere which is almost independent of the atmosphere that the primary target is sputtered in. Since reactive sputtering of the Aluminum target was applied, this requires an Ar/O_2 mixture. Gas separation between the main and auxiliary volumes is achieved by optimizing the aspect ratio (length/width) of the slits connecting these volumes. Additionally, the auxiliary targets are usually sputtered at elevated pressures of 5 Pa (main chamber: 0.4 Pa) leading to a strong purge effect which inhibits significant oxygen flow into the auxiliary volumes. The different atmospheres are surveyed by oxygen probes (Zirox) during the process to validate the required gas separation. The construction of all cathodes allows re-positioning of the magnet assemblies during operation to adjust the magnetic field. For

the auxiliary cathodes, also the balance of the magnet assembly can be changed during operation for optimum flexibility. Furthermore, the auxiliary cathodes can be adjusted in height, which is also true for the substrate stage. Consequently, all target-to-target and target-to-substrate distances can be adjusted during operation of the system. Here both distances have been fixed to 65 mm.
To obtain the W deposition profile and the co-deposition rates the planar rotating primary cathode has the advantage that it can easily be replaced by a substrate stage for film deposition from the auxiliary cathodes. Dynamic deposition onto a rotating substrate stage allows for designing the homogeneity masks that are utilized to tailor the deposition profile of auxiliary material onto the primary rotating cathode. Furthermore, the corresponding dynamic deposition rate and profile can be derived from the thickness of a dynamically deposited film.
Prior to deposition, the system is pumped down to $<2\times10^{-6}$ mbar by a Pfeiffer turbo-molecular pump with a pumping speed of 520 l/s (N_2) backed by a scroll pump (Edwards XDS 10). The sputter atmospheres are then controlled by MKS flow controllers. A 647C control unit is used for the main chamber (200 sccm Ar, 200 sccm N_2, 100 + 10 sccm O_2), while MKS type 250 controllers equipped with proportional valves are employed for the auxiliary volumes. Pressures are measured by MKS Baratron capacitance gauges in all volumes. All sputter cathodes can be operated simultaneously. Therefore, two Advanced Energy dual channel Pinnacle DC power supplies ($2 \times 2\times10$ kW) are available. One of these four channels is also powering a Melec SPIK 2000A pulsing unit that allows utilizing HiPIMS discharges with a peak output of 200 A at 1 kV. A single channel 5 kW Pinnacle Plus+ pulsed DC and a 1.2 kW 13.56 MHz Cesar RF power supply (Advanced Energy) are additionally available.
As a consequence of the complexity of the system the coater is fully computer-controlled by LabView-Software programmed in-house. This allows for automated discharge parameter analysis and characterization procedures as well as for complete sample data and process parameter data-mining for later review. Furthermore, feedback loops between plasma parameters and both output power and oxygen flow controls can be utilized to stabilize arbitrary working points of a reactive discharge with response times in the range of 10-20 ms. The superimposed output power and oxygen flow control algorithms allow for the fast stabilization of the hysteresis region also as a function of oxygen flow at constant mean output power or current, even with the comparatively slow mass flow controllers.

2.2. Thin film analysis

Deposition rates were deduced from film thicknesses that have been measured by x-ray reflectometry (XRR) with angstrom precision. Therefore a Philips X'Pert Pro MRD using Cu K_α radiation (λ = 1.54 Å) was utilized. The measured XRR patterns were simulated by the Philips WinGixa software to determine the thickness, mass density and interface roughness of the films. As a substrate, standard microscope slides (Menzel) were typically used for most of the films. For optical measurements, also Silicon and Quartz substrates have been utilized. The optical transmittance of the specimens was recorded employing a Perkin Elmer Lambda25 UV/VIS spectrometer in the spectral range of 190 – 1100 nm (1.13 – 6.53 eV) for an analysis of the Tungsten content in the deposited layers. This is possible since the band gap of WO_3 (3.1 eV, [18]) is significantly smaller than the band gap of amorphous Al_2O_3 (5.1 to 6.9 eV, [19]). Ellipsometry measurements utilizing a Woollam M2000-UI variable angle spectroscopic ellipsometer were performed for Al_2O_3 specimens on Silicon substrates to model the dielectric function (DF) of un-doped films. The elemental composition was measured for selected samples on Silicon substrates. Therefore, x-ray photoelectron spectroscopy (XPS), electron probe microanalysis (EPMA), and Rutherford backscattering spectrometry (RBS) measurements have been performed. For the XPS measurements, a PHI Quantum 2000 instrument with monochromatic Al K_α radiation was utilized. The background pressure in the analytical chamber was in the range of 10^{-9} mbar. Alternate measuring and sputtering cycles (2 keV Ar^+, 800 nA onto an area of 2×2 mm²) were performed for depth-profiling. Charging by the beam was compensated by an electron flood gun. Measurements of the O_{1s}, Al_{2p} and W_{4f} peaks were carried out with a resolution of 0.1 eV. The lowest elemental detection limit of this technique is about 0.01 at. % but varies with the film thickness and the species. For the RBS measurements a 1.4 MeV He^+-ion beam was utilized. The backscattered ions were detected at an angle of 170° with an energy

resolution of 1.29 keV. The signal was integrated for a fixed ion dose of 15 µC. Since the scattering cross section varies as the square of the nuclear charge of the target atom the technique is most sensitive for heavy elements such as Tungsten. Therefore it was possible to determine the W concentration in our films with an accuracy of 0.1 at. %.

3. Results and discussion

A reactive process was utilized to deposit Al_2O_3 films from a metallic Al target. The oxidation state of the target and the deposited films can be described by coupled rate laws in its simplest approximation. This requires knowledge of the reactive gas flow and partial pressure, the chemisorption of reactive gas at metallic surfaces, the erosion of metal and oxide compound from the target surface and the subsequent coverage of surfaces with the sputtered material [20][21]. The complexity of this process increases in a dynamic sputtering process characterized by a rotating target and the intentional change of its surface elemental composition by co-deposition from the auxiliary target. It has been shown by Depla et al. [15] that in a reactive sputtering process from a pure rotating Al target the transition between the metallic and compound target surface is affected by the rotation speed of the cathode. Rate laws under non-equilibrium conditions have to be considered in this case [22] as well as a realistic description of the oxidized target surface, where implantation plays an important role [17]. Developing an atomistic understanding of this process is challenging and is beyond the scope of this work. Here the experimental verification of sputter yield amplification in a newly developed serial co-sputtering setup is in the focus.

3.1. Process characteristics

To investigate the influence of Tungsten co-doping on the process characteristics, the behavior of the pure Aluminum target during reactive sputtering has to be investigated as a reference first. The most significant feature of the reactive sputtering process is the oxidation of the target surface as a function of oxygen flow. The oxidation state is correlated with the target voltage and the oxygen partial pressure which both change with oxygen flow. In this work the oxygen partial pressure is used to characterize the target oxidation state. In figure 2, this quantity is plotted as a function of oxygen flow for two different rotation speeds of the Aluminum target without Tungsten co-doping. For both speeds, the transition between metallic and oxidized states is characterized by an abrupt change in the oxygen partial pressure at characteristic oxygen flows. Furthermore, forward (metallic -> oxidized) and reverse (oxidized -> metallic) transitions during increasing and decreasing oxygen flow, respectively, occur at different flows. This hysteresis is typical for reactive sputtering [20][21].

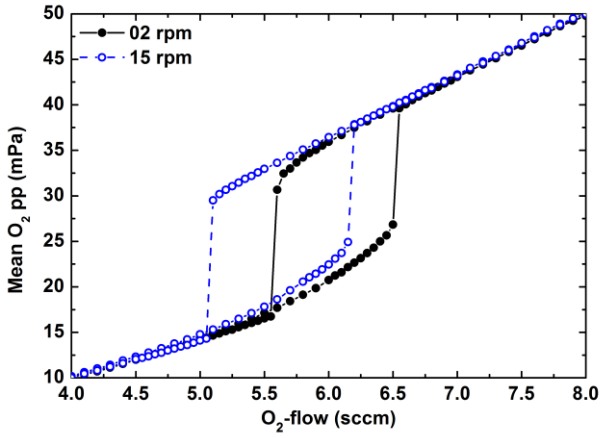

Figure 2. Characteristic of the reactively sputtered Aluminum target as a function of the oxygen flow. A change of the characteristic behavior with rotation speed is shown. At higher rotation speed both the forward and reverse transition shift to lower oxygen flows and the hysteresis window is slightly broadened.

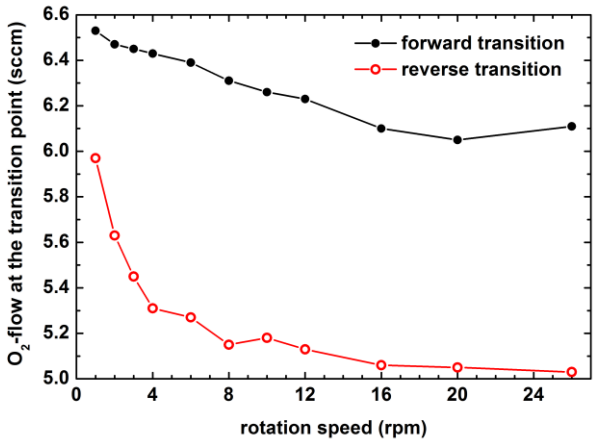

Figure 3. Forward and reverse transition flows of reactively sputtered Aluminum as a function of rotation speed. With increasing rotation speed of the Aluminum target both the forward and reverse transition flows shift to lower values and the width of the hysteresis (distance between forward and reverse transition flows) increases.

It is apparent that the oxygen flow at the transition point depends on the rotation speed of the target, since the hysteresis curves shift upon changing rotation speed. This is shown in figure 3, where only the forward and reverse transition flows are plotted as a function of rotation speed. From this plot it is evident that the width of the hysteresis increases with rotation speed, especially for low speeds. At high speeds saturation apparently occurs. Additionally, there is an overall shift of the hysteresis towards lower oxygen flows at high rotation speeds. These findings agree with results for the reactive sputtering of a cylindrical Aluminum target [15]. Smith et al. observed the shift in the transition regime in reactive sputtering processes from a dual rotatable cathode [23]. The dependence of the hysteresis upon rotation speed was also predicted in simulations performed by Kappertz et al. [22] and was mainly attributed to chemisorption of oxygen on the target surface. There it has been argued that an increase in rotation speed results in a decrease in oxygen consumption, which takes place at the target as well as at the receiving areas (chamber wall, shields, and substrates). The total receiving area is much larger than the active area of the target and has a larger effect on the behavior of the reactive sputtering process. With increasing rotation speed of the target, the erosion time per cycle of a specific area within the erosion trace decreases. This results in a larger remaining oxygen coverage after passing the plasma. Hence, the working points shift towards the oxidized mode, which also implies that less metal is deposited onto the receiving areas. Less oxygen would therefore be consumed leading to a shift of the transition flows towards lower values. The close correspondence of our results with the data published by Depla [15] furthermore indicates that the characteristic behavior of a cylindrical and a planar rotating target is very similar in terms of the process behavior during reactive sputtering. Recent investigations of Depla et al. [17] have shown that the target characteristic of a rotatable target is also affected by material deposition onto the target during sputtering especially at low oxygen flows.

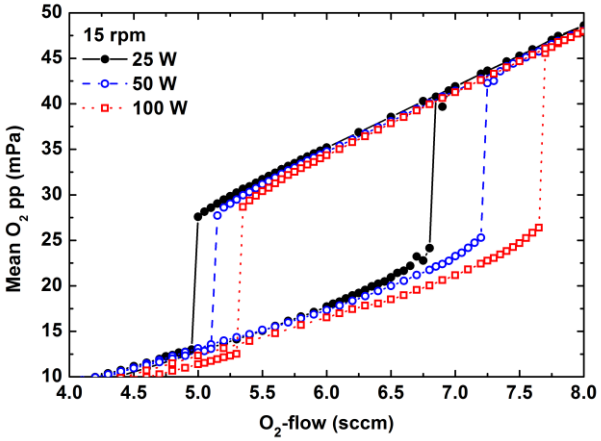

Figure 4. Characteristics of reactively sputtered W-co-doped Aluminum for different sputtering powers $\mathbf{P_W}$ of the Tungsten target (25, 50 and 100 W) at a constant rotation speed of 15 rpm of the Aluminum target. The hysteresis window broadens and shifts to higher oxygen flows with increasing discharge power of the Tungsten target.

Subsequently, the transition characteristics have been studied with additional Tungsten co-doping of the Aluminum target. First, the effect of doping is demonstrated for a fixed rotation speed of 15 rpm, which is depicted in figure 4. There the oxygen partial pressure is plotted as a function of oxygen flow for different doping concentrations. Doping is controlled by the power P_W (25, 50 and 100 W) applied to the Tungsten cathode, which is proportional to the dynamic deposition rate of Tungsten of about $7.25 \cdot 10^{-5}$ nm/(W·s). It is obvious that the transition characteristics of the Al-target are significantly altered by Tungsten doping. As can be seen from figure 4, with increasing P_W the transition regime is widened and shifts to higher oxygen flows. As displayed in figure 5, the dependence on the rotation speed has notably changed.

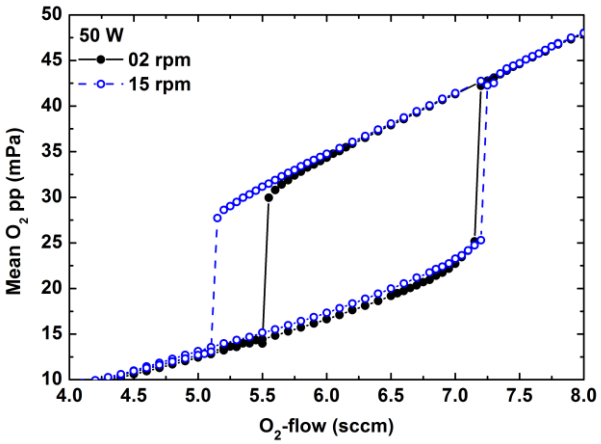

Figure 5. Characteristics of reactively sputtered W-co-doped Aluminum for different rotation speeds of the primary target (2 and 15 rpm) and for a constant co-sputtering power of $\mathbf{P_W}$ = 50 W. With increasing rotation speed the forward transition shifts to slightly higher oxygen flows whereas the reverse transition clearly shifts to lower oxygen flows. Hence, the width of the hysteresis window is significantly increased.

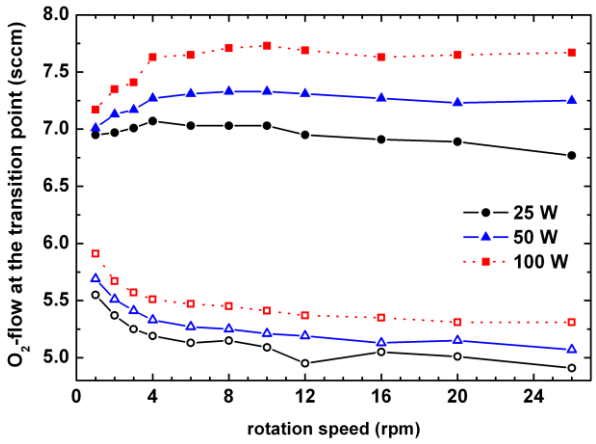

Figure 6. Forward (closed symbols) and reverse transition flows (open symbols) of reactively sputtered W-co-doped Aluminum as a function of rotation speed. This characteristic is displayed for different co-sputtering discharge powers P_W of 25, 50 and 100 W. The most significant difference with respect to the behavior of the un-doped Aluminum target is the increase of the forward transition flow with increasing rotation speed.

In contrast to the un-doped Aluminum target the forward transition does not seem to change to lower flows upon increasing rotation speed. This fact is clearly depicted in figure 6, where the forward and reverse transition flows are plotted as a function of rotation speed for different doping concentrations adjusted by P_W. The overall shift of the forward transition to higher oxygen flows in comparison with the un-doped target (cf figure 3) can be understood considering the increase in deposition rate discussed in the following section. Since the oxygen consumption is directly proportional to the erosion rate, there is an increase upon doping with Tungsten. The trends observed in the reverse transition are more difficult to explain. The fact that the reverse flows exhibit a general increase with increasing doping concentration (figure 6) may be interpreted in terms of the increased erosion rate as well. However, this trend is not entirely consistent with the un-doped case especially for low rotation speeds (cf figure 3). A very interesting observation is that the forward transition flow significantly increases as a function of rotation speed, specifically at low speeds. There seems to be a small maximum around 8-10 rpm after which there is a slight decrease again. This is in strong contrast to the un-doped case, where the forward transition flow is a monotonically decreasing function of the rotation speed. We will first discuss the sputter yield amplification and the corresponding concentration of Tungsten in the films deposited before coming back to this point**.**

3.2. Sputter yield amplification and film properties

3.2.1. Sputter yield amplification. In order to determine the deposition rate and film properties, samples have been deposited at different working points (oxygen flows). Specimens used to determine the deposition rate have been deposited onto standard microscope slides whereas specimens used for the determination of the elemental composition were deposited onto Silicon substrates. Figure 7 displays the deposition rate as a function of the oxygen partial pressure in the main chamber volume. The rotation speed of the Aluminum target has been kept fixed at 2 rpm for these series. The film thickness and density has been measured by XRR, whereas the mass density has not changed significantly for different doping concentrations of W. The rates were determined from the layer thickness and the known deposition time. The upper viewgraph depicts the deposition rates for both pure Aluminum and for different concentrations of Tungsten. The Tungsten concentration is expressed in terms of the discharge power P_W. This quantity is proportional to the dynamic deposition rate of Tungsten onto the rotating Aluminum target. The rates for

pure Aluminum have been determined twice, before and after sputtering with additional Tungsten doping, to confirm that target aging does not lead to a drift in rate. In the metallic mode the deposition rate is high and can be significantly increased by co-doping of the primary target. A considerable increase in deposition rate is already apparent for P_W = 25 W. A maximum increase of about 50 % is obtained for P_W = 100 W. With increasing Tungsten concentration the deposition rate saturates. This is evidence that the sputter yield amplification is specifically pronounced for very low doping concentrations. In the oxide mode the deposition rates are about one order of magnitude lower than in metallic mode. The lower viewgraph in figure 7 displays a magnification of the corresponding regime. The relative increase in deposition rate in the oxide mode ranges from about 40 % for P_W = 25 W to about 80 % for P_W = 100 W.

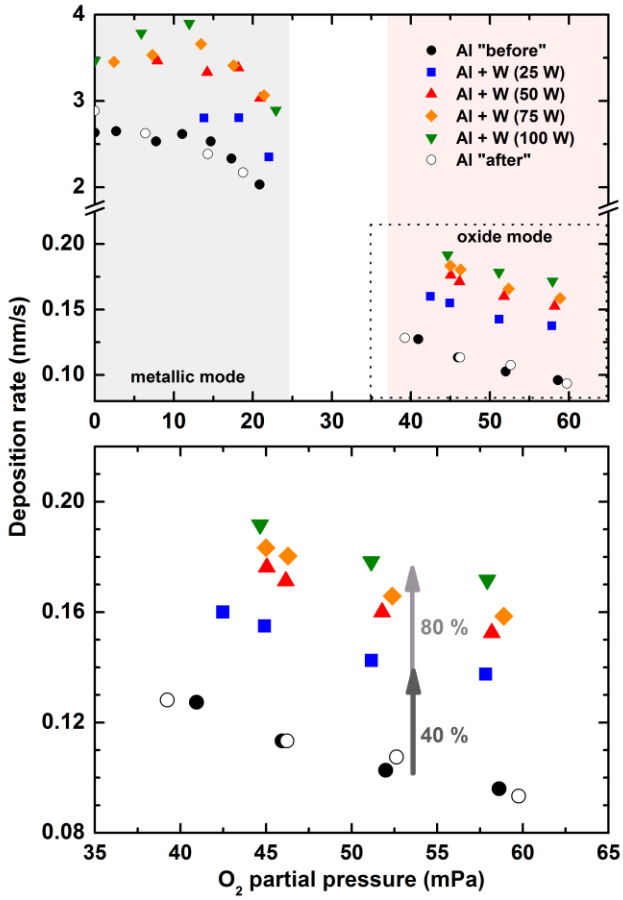

Figure 7. Deposition rates of reactively sputtered Aluminum as a function of the oxygen partial pressure for a constant rotation speed of the primary target of 2 rpm. The co-sputtering discharge power and therefore the deposition rate of Tungsten has been varied from P_W = 0 W to P_W = 100 W, where 0 W correspond to the un-doped Aluminum target. The lower graph depicts a magnification of the compound regime (oxide mode). There is a clear increase in the deposition rates of Al and Al_xO_y films upon Tungsten doping. The most significant increase in deposition rate in oxide mode occurs already for the lowest doping concentration at P_W = 25 W. For larger Tungsten concentrations the increase in deposition rate saturates.

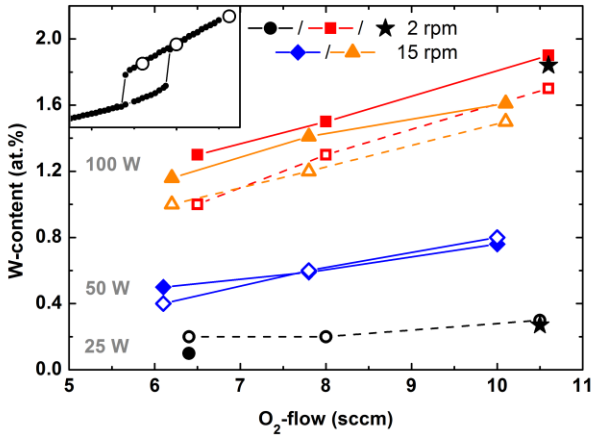

Figure 8. Measured Tungsten concentration in W-co-doped Al_2O_3 layers deposited at different working points of the oxidic mode at two different rotation speeds (2 and 15 rpm) and different co-sputtering power P_W (25, 50 and 100 W). Full symbols: XPS, open symbols: EPMA, stars: RBS.

3.2.2. Incorporation of Tungsten into the films. To investigate the efficiency of the sputter yield amplification, the amount of Tungsten incorporated into the deposited films has been measured. From the XRR measurements performed to determine the film thickness it was already deduced that the concentration of Tungsten must be small in the films since no change in mass density was detected. This assumption has been confirmed by subsequent XPS, EPMA and RBS measurements on selected specimens. The Tungsten concentration is depicted in figure 8 for specimens deposited at different rotation speeds of the Aluminum target, at different sputtering powers P_W of the Tungsten target and at different working points (cf also table 1). As depicted in the inset, the selected oxygen flows correspond to working points at the edges of the hysteresis (oxidic "side" of the forward and reverse transition flows) and to an oxygen flow far in the oxide mode. It is evident that the XPS, EPMA and RBS results agree very well. They show very low Tungsten contents even for the largest sputtering power P_W of the Tungsten target. The Tungsten concentration does not exceed 2 at. %. The Tungsten content generally decreases with decreasing oxygen flow for fixed P_W. This is a consequence of the larger Al sputter yield with respect to the deposited amount of W at low oxygen flows. It is noteworthy that significant sputter yield amplifications are observed already at P_W = 25 W where Tungsten incorporation is hardly detectable. Upon increasing P_W the corresponding concentration in the films increases stronger than linear. At the same time the sputter yield amplification converges as P_W increases, which is demonstrated in figure 7. This is in agreement with simulations [16] which show that the Al sputter yield is maximal at about 2-3% of W in Al and decreases for larger concentrations. This is because in serial co-sputtering an increase in the W concentration correlates with an increase of the thickness of the W layer deposited each turn. For an increasing layer thickness, the implantation efficiency decreases as a consequence of limited ion range (implantation depth). Hence the amount of Tungsten that is implanted into the Aluminum target is limited to a small fraction which is not proportional to the overall surface coverage with Tungsten. Therefore there is a concentration limit above which a further increase in coverage of the Aluminum target by Tungsten merely adds to the W concentration in the film but no longer increases the sputter yield.

To investigate how the physical properties of the Al_2O_3 specimens change upon doping with Tungsten, optical measurements have been performed. By utilizing spectroscopic ellipsometry (0.73 – 5.13 eV) as well as reflectance and transmittance measurements (1.13 – 6.53 eV), at first an optical model was developed for the Quartz, pure Al_2O_3 and WO_3 films. For the ellipsometry measurements Silicon was used as a substrate, whereas Quartz was employed to record the R+T spectra. The optical spectra were modeled using the Scout software. The dielectric function of WO_3 has been modeled by describing the fundamental absorption by an OJL model. An additional harmonic oscillator has been placed in the UV to model a

slightly non-constant offset of the dielectric background. The Al_2O_3 has been modeled by utilizing a Tauc-Lorentz density of states to describe the fundamental absorption [24][24]. The weak order of the amorphous system was taken into account by an additional absorption exponentially decaying into the forbidden region. This was modeled by an oscillator with Gaussian shape. That combination turned out to give slightly better fits than with a conceptually similar OJL model [25]. Spectra of pure Al_2O_3 and WO_3 as well as for doped Al_2O_3:W films are shown in figure 9.

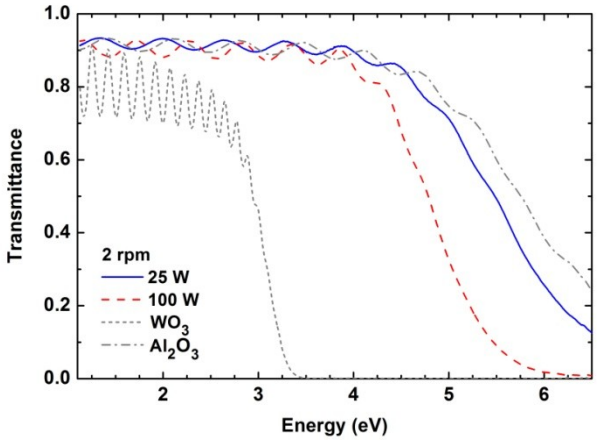

Figure 9. Optical transmittance of pure Al_2O_3, pure WO_3 and co-doped Al_2O_3:W films. Upon doping the absorption edge shifts to lower energies. This shift increases with doping concentration (discharge power of the Tungsten target).

Incorporation of Tungsten results in an additional absorption shifting the absorption edge towards lower photon energies in Al_2O_3:W. In a first attempt an effective medium theory (Bruggeman) was utilized to model the Al_2O_3:W films as a homogeneous mixture of Al_2O_3 and WO_3 with the dielectric functions determined for the pure films. It was found, however, that this model cannot adequately describe the optical spectra of Al_2O_3:W. Therefore, the incorporated Tungsten has been treated as an impurity instead. To determine the shape of the absorption band correlated with the impurity, 12 specimens with different Tungsten concentrations have been modeled simultaneously where only differences in film thickness and in the strength of this specific absorption band were allowed for the different specimens that were otherwise described by the same fixed dielectric function of Al_2O_3. It has been found that the Tungsten impurities constitute a broad absorption band at an energy just below the fundamental absorption of the Al_2O_3, as shown in figure 10. Figure 11 demonstrates how this absorption band affects the transmittance of the Al_2O_3:W films as a function of Tungsten concentration. The correlation between the strength of the additional absorption band and the Tungsten concentration was derived from the modeled absorption. The strength of the absorption band related to the Tungsten impurities clearly increases with the Tungsten incorporation as determined by EPMA measurements. The strength of this absorption has then been renormalized by a constant proportionality factor to match the results of the EPMA measurements.

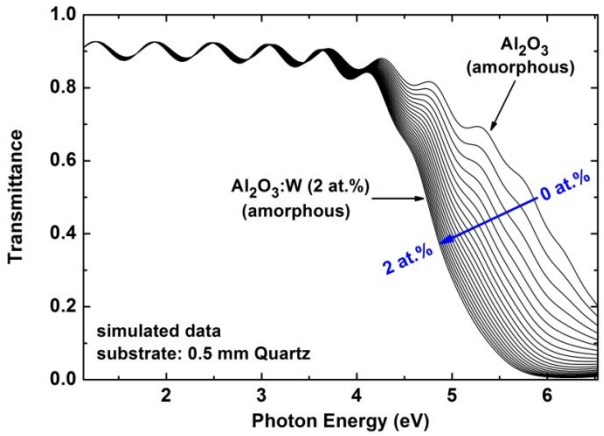

Figure 10. Simulation of optical transmittance of co-doped Al_2O_3:W films. The underlying dielectric function has been derived from modeling the specimens described in table 1. The simulation depicts the characteristic shift of the absorption edge of Al_2O_3 upon increasing the Tungsten concentration in the film from 0 at% to 2 at%.

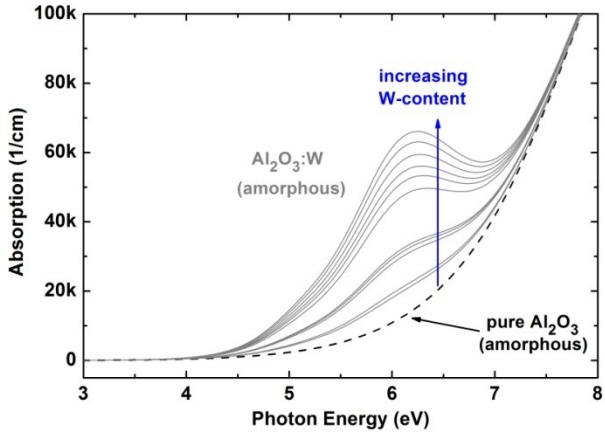

Figure 11. Optical absorption coefficient derived from the modeled dielectric function of Al_2O_3:W films. Dashed line: pure Al_2O_3. Grey solid lines: Al_2O_3:W with different Tungsten concentrations (cf table 1). From the modeling results it can be deduced that the Tungsten incorporated in Al_2O_3 forms a broad impurity band at an energy level close to the onset of the Al_2O_3 fundamental absorption.

The renormalized absorption is shown in figure 12 and is interpreted as the atomic concentration of Tungsten in the films. This is based on the assumption that in the concentration range investigated the correlation between the impurity concentration and the corresponding optical absorption is linear. In figure 13 it is demonstrated that the incorporation of Tungsten leads to a noticeable but small change in the refractive index of the specimens in the visible regime. Table 1 shows a comparison of the results from

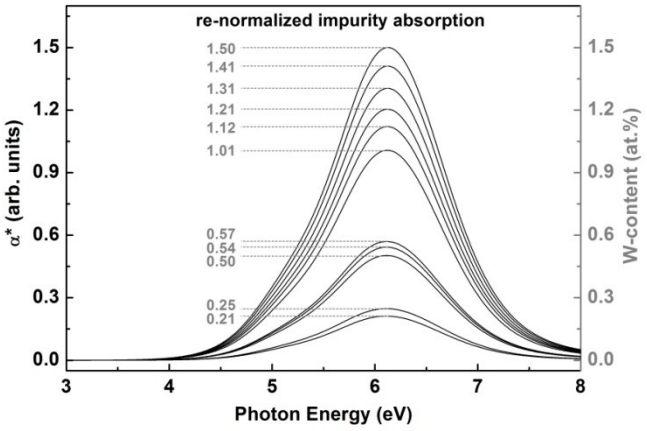

Figure 12. Re-normalized impurity fraction of the absorption coefficient in Al_2O_3:W. The absorption background of the pure Al_2O_3 (cf figure 11) has been subtracted such that the remaining absorption can be attributed to the Tungsten impurity band solely. In a linear approach for the correlation between the optical absorption and the impurity concentration in the investigated range of 0-2 at%, the impurity absorption has been re-normalized to match the EPMA data.

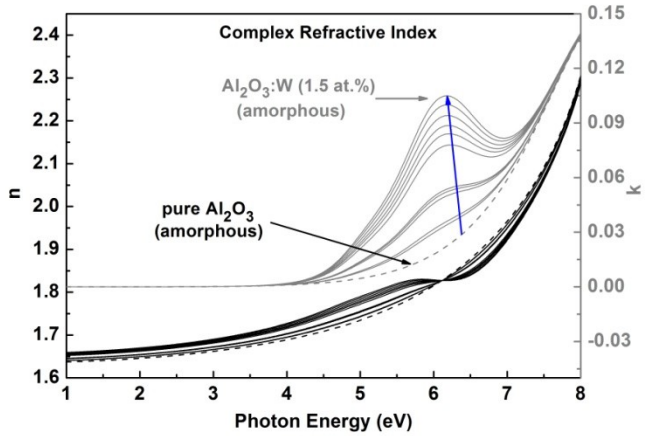

Figure 23. Complex refractive index of the co-doped Al_2O_3:W films modeled (cf table 1 for sample details). It is apparent that in the visible range the effect of doping on the refractive index is very small.

EPMA measurements and the optical simulation. The good qualitative agreement with the EPMA results shows that the Tungsten incorporation can be determined by optical measurements with good accuracy. This is important since it facilitates an online rate and quality control of Al_2O_3:W coatings fabricated with additional doping by serial co-sputtering. As for the EPMA results, a non-linear increase of Tungsten concentration, i.e. of the strength of the additional absorption band, is evident from the optical modeling. This also supports the decreased efficiency of the sputtering yield amplification for larger Tungsten concentrations.

The increase in deposition rate and the low Tungsten content in the deposited layers confirm the sputter yield amplification of Al_2O_3. These experimental results are in good agreement with previous simulations where we have shown an increase of the Al partial sputter yield in oxide mode by 80 % utilizing a

concentration of 2 at. % W in the Al-target. Additionally, at an oxygen pressure of 100 mPa these simulations have predicted a maximum partial sputter yield of Al of about 150 % as compared to an un-doped target for a Tungsten concentration of 10 at. %. [16]

Table 1. Tungsten concentration in Al_2O_3 layers for different rotation speeds (2 and 15 rpm) of the Aluminum target, different sputtering powers P_W of the Tungsten target (25, 50 and 100 W), and different working points (oxygen partial pressures). The choice of working points is further elucidated in figure 8. The chemical composition has been determined by EPMA. Trends in the measured Tungsten concentrations compare well with the values deduced from the corresponding absorption in the modeled dielectric function (DF).

rpm	P (W)	O_2 p.p. (mPa)	Deposition rate (nm/s)	W-content EPMA (at.%)	W-content DF (at.%)
2	25	34.3	**0.191**	**0.2**	**0.21**
2	25	44.5	**0.149**	**0.2**	**0.25**
2	25	59.4	**0.128**	**0.3**	**0.25**
15	50	33.7	**0.230**	**0.4**	**0.50**
15	50	45.0	**0.164**	**0.6**	**0.54**
15	50	59.8	**0.142**	**0.8**	**0.57**
15	100	33.5	**0.257**	**1.0**	**1.01**
15	100	44.7	**0.194**	**1.2**	**1.21**
15	100	59.6	**0.169**	**1.5**	**1.31**
2	100	34.5	**0.248**	**1.0**	**1.12**
2	100	44.1	**0.189**	**1.3**	**1.41**
2	100	60.2	**0.163**	**1.7**	**1.50**

3.3. Dynamics of reactive serial co-sputtering

As has been discussed before, the process characteristics significantly change upon doping the Aluminum target with Tungsten. This is evident from the functional dependence of the forward transition oxygen flow on the rotation speed of the Al target (cf figures 3 and 6). To unravel this feature, the following observations and facts will be discussed:

1. In [16] (figure 1 therein) it has been demonstrated that there is an optimum doping concentration where the rate enhancement exhibits a maximum. At higher doping levels the SYA becomes less efficient and instead the dopant rather contributes to the film composition only. While these calculations have been performed for a homogeneously doped target, results published by Carlsson et al [13] are more closely comparable with serial co-sputtering. There it was shown that for a Tungsten bi-layer on an Aluminum surface a variation in the bombarding ion dose results in different sputter yields. Moreover, a clear dependence of the partial Aluminum sputter yield was also shown for the thickness of the Tungsten layer. An optimum sputter yield enhancement was found for a specific Tungsten layer thickness. The main reason for that is a correlation between the bi-layer thickness and the implantation depth (ion range). This means that for large bi-layer thicknesses the doping material is sputtered away instead of being implanted to increase the erosion rate of the target material below. This fact is in agreement with the findings in [16] that the efficiency of doping in terms of the sputter yield amplification saturates upon increasing the Tungsten doping level.
2. In the serial co-sputtering process the surface areal density of the deposited doping material is a function of the rotation speed of the rotatable target (if P_W = const.) and is also subject to a

gradual change while passing through the primary erosion area. This has been simulated qualitatively for a process in compound mode (figure 14). The upper and lower graphs show the sputter yield of the Aluminum and the Tungsten along the full width of the primary erosion trace, respectively. The simulation follows a fixed point on the target surface that enters the primary erosion area at 0 and leaves at 1 (see abscissa in figure 14). For a low W-content and a high rotation speed (0.1 Hz) the Aluminum yield enhancement is constantly high across the full width of the erosion area. However, if the rotation speed is decreased (0.01 Hz) it is evident that the Tungsten is rather sputtered away upon entrance into the erosion zone and the yield enhancement quickly drops towards the end of the erosion area. If also the W-content is increased Tungsten is primarily sputtered upon entrance and the Aluminum yield is even lower than optimum. The Aluminum yield also quickly drops towards the end of the erosion area. In summary, the mean Aluminum yield enhancement (integral over the entire erosion area) has a clear maximum for high rotation speeds and low W-contents.

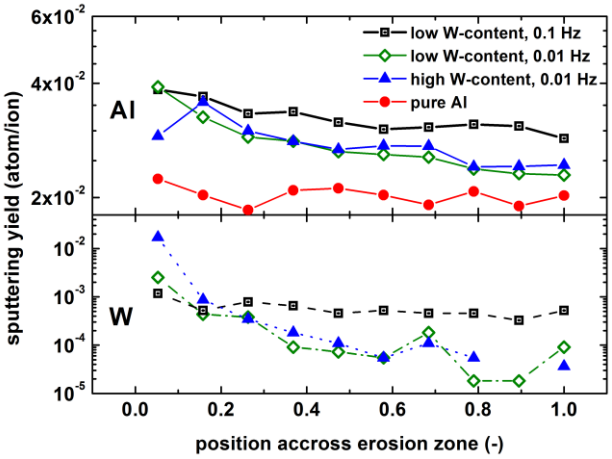

Figure 14. TRIDYN simulation of the evolution of the sputtering yields of Al and W across the erosion zone in direction of rotation for reactive sputtering (100 mPa O_2). A fixed point on the rotatable target surface is followed which enters the primary erosion zone at point "0" on the abscissa and leaves at "1". The upper viewgraph shows the partial sputtering yields of Al (straight lines) for different rotation speeds and W-contents. The lower viewgraph displays the corresponding yields of W (doted lines). It is evident that the Aluminum yield enhancement is constantly high across the full erosion zone only for low W-concentrations and high rotation speeds. Lower speeds primarily result in sputtering away most of the Tungsten bi-layer upon entering the erosion zone, which decreases the average Al yield enhancement. An increase of the W-content cannot compensate for this, since this merely results in a larger fraction of W sputtered upon entering the erosion zone.

In table 1 there is evidence for a correlation between the film stoichiometry and the rotation speed at fixed P_W. It is evident that at P_W = 100 W the amount of incorporated Tungsten in Al_2O_3:W slightly decreases upon increasing the rotation speed from 2 to 15 rpm if specimens are compared that have been deposited at similar oxygen partial pressures. This finding coincides with a slightly higher deposition rate at 15 rpm. Even though this supports the above-mentioned interpretations the authors are aware of the fact that there is limited comparability of films sputtered at identical oxygen partial pressures in a case where the process behavior (i.e. the position of the forward and reverse flows) is clearly shifted. However, additional evidence that there is a pronounced change in the mean sputter yield as a function of cathode rotation speed is the fact that the Tungsten content in the deposited films disproportionally increases with P_W. This

can be directly read from figure 8 which proves that the Tungsten concentration increases stronger than linear with the target doping concentration, which has been confirmed to change exactly linear with P_W. That observation is hence unambiguous proof that upon increasing P_W from 50 W to 100 W the SYA already becomes less efficient in terms of the discussion above (points 1 and 2). It is therefore plausible that the efficiency is very sensitive to changes in the rotation speed within the covered range of parameters.

From the facts and the statements discussed above we can now understand the behavior of the forward transition flow shown in figure 6. Although on average the Tungsten coverage of the Aluminum target is not a function of rotation speed, there is a comparatively thicker Tungsten layer deposited during each revolution at low speed. Consequently, when entering the primary erosion zone a thick layer has to be gradually removed. This means that for a significant fraction of the primary erosion zone the Tungsten coverage is larger than the thickness which would correspond to an optimum implantation and rate enhancement efficiency. In that case, a large fraction of the Tungsten is just sputtered away from the target surface and incorporated into the film instead of being implanted to enhance the erosion rate. Hence, due to that loss of efficiency the average erosion rate at low rotation speeds is lower than at high speeds when the erosion becomes more homogeneous along the primary erosion area. In other words, the erosion rate increases as a function of rotation speed and saturates when the erosion profile becomes comparably homogeneous. Hence, for reasons that have already been mentioned the forward transition flow also has to asymptotically increase with rotation speed. Interestingly, for the forward transition flow this contribution of the erosion rate even compensates the typically decreasing trend observed for the un-doped target. For the reverse transition this is not the case. However, while for the un-doped target the reverse flow decreases by about 1 sccm (cf figure 3) with increasing rotation speed, the corresponding decrease for the doped target is smaller by about 0.5 sccm (cf figure 6). This is evidence for the influence of the change in erosion rate also on the reverse transition flows.
The conclusions drawn on the correlation between the W coverage of the Aluminum target surface and the implantation efficiency of W into the Aluminum target are in line with simulations published by Carlsson et al. [13] and Kubart et al [16]. From figure 6 it is evident that homogeneous erosion and hence an optimum rate enhancement is reached at a rotation speed of about 8 rpm for a fixed Tungsten sputtering power.

4. Conclusions

For Al_2O_3 films deposited by serial co-sputtering the deposition rate increased by up to 80 % upon co-doping with Tungsten. The amount of Tungsten incorporated into the films is of the order of 1 at. % only. The efficiency of the sputter yield amplification saturates with increasing W concentration. This is due to the fact that the fraction of Tungsten implanted into the Aluminum target is limited. Surplus Tungsten is sputtered away and incorporated into the growing film. There is evidence that this behavior also affects the process dynamics as a function of rotation speed of the cathode. Optical spectra of Al_2O_3:W films have been measured and subsequently modeled. It has been shown that the incorporated Tungsten can be described by an additional impurity band in the amorphous Al_2O_3 matrix. From the modeled DF the concentration of Tungsten can be derived by renormalizing the corresponding impurity absorption. Hence, optical methods could be utilized for online monitoring of both the film thickness (i.e. the rate enhancement) and the Tungsten concentration in the coatings.

Acknowledgments
Financial support by the Volkswagen Foundation (project COSMOS, Contract No. I/83 234) and the DFG (Wu 243/18) is gratefully acknowledged. We thank B. Holländer and the operators at Peter Grünberg Institut 9, Forschungszentrum Jülich for providing access to the Tandetron ion accelerator.

References:

[1] Ngaruiya J M, Kappertz O, Mohamed S H, and Wuttig M 2004 Structure formation upon reactive direct current magnetron sputtering of transition metal oxide films *Appl. Phys. Lett.* **85** 748
[2] Bräuer G, Szyszka B, Vergöhl M and Bandorf R 2010 Magnetron Sputtering – Milestones of 30 Years *Vacuum* **84**
[3] Severin D, Kappertz O, Kubart T, Nyberg T, Berg S, Pflug A, Siemers M and Wuttig M 2006 Process stabilization and increase of the deposition rate in reactive sputtering of metal oxides and oxynitrides *Appl. Phys. Lett.* **88** 161504
[4] Severin D, Kappertz O, Nyberg T, Berg S, Pflug A and Wuttig M 2009 Increase of the deposition rate in reactive sputtering of metal oxides using a ceramic nitride target *J. Appl. Phys.* **105** 093302
[5] Billard A, Mercs D, Perry F and Frantz C 1999 Influence of the target temperature on a reactive sputtering process *Surf. Coat. Technol.* **116-119** 721-26
[6] Mercs D, Perry F and Billard A 2006 Hot target sputtering: A new way for high-rate deposition of stoichiometric ceramic films *Surf. Coat. Technol.* **201** 2276-81
[7] Chau R Y, Ho W S, Wolfe J C and Licon D L 1996 Effect of target temperature on the reactive d.c.-sputtering of silicon and niobium oxides *Thin Solid Films* **287** 57-64
[8] Sarakinos K, Alami J, Klever C and Wuttig M 2008 Process stabilization and enhancement of deposition rate during reactive high power pulsed magnetron sputtering of zirconium oxide *Surf. Coat. Technol.* **202** 5033-35
[9] Anders A 2010 Deposition rates of high power impulse magnetron sputtering: Physics and economics *J. Vac. Sci. Technol. A* **28** (4)
[10] Berg S, Barklund A M, Gelin B, Nender C and Katardjiev I 1992 Atom assisted sputtering yield amplification *J. Vac. Sci. Technol. A* **10** (4)
[11] Berg S, Barklund A M, Nender C, Katardjiev I and Barankova H 1992 Sputter erosion amplification *Surf. Coat. Technol.* **54/55** 131-35
[12] Belkind A, Orban Z, Berg S and Carlsson P 1993 Serial cosputtering of some metal alloys: Enhancement of partial sputtering yields of light metals *J. Vac. Sci. Technol. A* **11** (2)
[13] Carlsson P, Berg S, Belkind A and Katardjiev I V 1993 Serial cosputtering of metals: modeling of sputtering from a periodically codeposited surface *Surf. Coat. Technol.* **61** 287-92
[14] Berg S and Katardjiev I V 1999 Preferential sputtering effects in thin film processings *J. Vac. Sci. Technol. A* **17** (4)
[15] Depla D, Haemers J, Buyle G and De Gryse R 2006 Hysteresis behavior during reactive magnetron sputtering of Al2O3 using a rotating cylindrical magnetron *J. Vac. Sci. Technol. A* **24** (4)
[16] Kubart T, Nyberg T, Pflug A, Siemers M, Austgen M, Koehl D, Wuttig M and Berg S 2010 Modelling of sputtering yield amplification effect in reactive deposition of oxides *Surf. Coat. Technol.* **204** 3882-86
[17] Depla D, Li X Y, Mahieu S, Van Aeken K, Leroy W P, Haemers J, De Gryse R and Bogaerts A 2010 Rotating cylindrical magnetron sputtering: Simulation of the reactive process *J. Appl. Phys.* **107** 113307
[18] Subrahamanyam A, Karuppasamy A 2007 Optical and electrochromic properties of oxygen sputtered tungsten oxide (WO3) thin films *Sol. Energy Mater. Sol. Cells* **91** 266-74
[19] Momida H, Hamada T, Takagi Y, Yamamoto T, Uda T and Ohno T 2006 Theoretical study on dielectric response of amorphous alumina *Phys. Rev. B* **73** 054108

[20] Berg S, Blom H-O, Larsson T and Nender C 1986 Modeling of reactive sputtering of compound materials *J. Vac. Sci. Technol. A* **5** (2)
[21] Berg S and Nyberg T 2005 Fundamental understanding and modeling of reactive sputtering processes *Thin Solid Films* **476** 215-30
[22] Kappertz O, Nyberg T, Rosén D and Berg S 2004 Influence of Rotating Magnets on Hysteresis in Reactive Sputtering *47th Annual Technical Conference Proceedings* Dallas, TX USA
[23] Smith A W, Butcher N G and Walker D 2002 Reactive Sputtering from a Dual Rotatable Cathode for SiO2, Si3N4 and SiOxNy coatings onto Flexible Substrates *45th Annual Technical Conference Proceedings* Braunschweig
[24] Jellison Jr G E and Modine F A 1996 Parameterization of the optical functions of amorphous materials in the interband region *Appl. Phys. Lett.* **69** (3) 371
[25] O'Leary S K, Johnson S R and Lim P K 1997 The relationship between the distribution of electronic states and the optical absorption spectrum of an amorphous semiconductor: An empirical analysis *J. Appl. Phys.* **82** (7) 3334-40